Hindawi
Advances in Mathematical Physics
Volume 2020, Article ID 8121295, 11 pages
https://doi.org/10.1155/2020/8121295

Research Article

Non-Fourier Heat Conduction of a Functionally Graded Cylinder Containing a Cylindrical Crack

Jiawei Fu,[1] **Keqiang Hu**,[2] **Linfang Qian**,[1] **and Zengtao Chen**[3]

[1]*Department of Mechanical Engineering, Nanjing University of Science and Technology, Nanjing, Jiangsu 210094, China*
[2]*Department of Chemical and Materials Engineering, University of Alberta, Edmonton, AB T6G 1H9, Canada*
[3]*Department of Mechanical Engineering, University of Alberta, Edmonton, AB T6G 1H9, Canada*

Correspondence should be addressed to Jiawei Fu; jwfu@njust.edu.cn

Received 27 September 2019; Revised 13 November 2019; Accepted 19 November 2019; Published 1 February 2020

Academic Editor: P. Areias

The present work investigates the problem of a cylindrical crack in a functionally graded cylinder under thermal impact by using the non-Fourier heat conduction model. The theoretical derivation is performed by methods of Fourier integral transform, Laplace transform, and Cauchy singular integral equation. The concept of heat flux intensity factor is introduced to investigate the heat concentration degree around the crack tip quantitatively. The temperature field and the heat flux intensity factor in the time domain are obtained by transforming the corresponding quantities from the Laplace domain numerically. The effects of heat conduction model, functionally graded parameter, and thermal resistance of crack on the temperature distribution and heat flux intensity factor are studied. This work is beneficial for the thermal design of functionally graded cylinder containing a cylindrical crack.

1. Introduction

Cylindrical composite structures are widely used in engineering, and the interfaces in the composites are key parts but at the same time weak regions, considering that these weak regions are generally subjected to various damages such as debonding or cracking. When a cylindrical interface debonds, the crack may occupy the whole angular range which is called a cylindrical crack [1]. Functionally graded (FG) materials have received considerable attention in engineering fields due to the fact that FG materials possess gradual change in composition and microstructure and have continuously spatial variations in thermal and mechanical properties. The application of FG materials can improve the bonding strength and toughness and reduce the probability of thermomechanical problems caused by the mismatch of material properties. Due to their important characteristics, FG materials found various applications, such as: inner walls of nuclear reactor, pressure vessels, thermal barrier coatings for combustion chambers, heat exchanger tubes, etc., [2]. The common fabrication technologies for producing FG bulk materials include powder metallurgy, centrifugal casting, tape casting, and additive manufacturing [3]. And, it has been found that embedded microcracks or cracks are prone to occur during the manufacture process of structures or in their service [4–6]. For instance, cylindrical cracks may initiate along the interface of fiber and matrix in the fiber reinforced composite cylinders [7]. Thus it is a significant design issue to study the thermal or mechanical fracture behaviors of FG structures [8, 9].

Great efforts have been made to investigate the fracture behavior of FG materials under mechanical and/or thermal loading [10–15]. Jin [16] studied the singular crack-tip fields in non-homogeneous body under thermal stress and pointed out that the stress intensity factors (SIFs) were still applicable in fracture problems of FG materials. Li and Weng [17] investigated the dynamic problem of a cylindrical crack in a functionally graded interlayer bonded by two dissimilar, homogeneous cylinders under torsional impact loading. Jin and Paulino [18] studied a crack in a viscoelastic strip of a FG material under tensile loading and obtained both mode I and mode II SIFs and the crack opening/sliding displacements. Feng et al. [19] considered the problem of a cylindrical crack in the non-homogeneous, interfacial zone in a composite loaded by torsional impact. The plane, thermo-mechanical behavior of a crack in a viscoelastic FG material coating with arbitrary material properties bonded to homogeneous

substrate has been studied by Cheng et al. [20]. The problem of a cylindrical interface crack in a hollow, functionally graded cylinder under static torsion has been studied by Shi [21], and the coupled effects of geometrical, physical, and functionally graded parameters on the interfacial fracture behavior have been demonstrated by numerical results. Zhang et al. [22] analyzed a thermal shock problem of an elastic strip made of functionally graded materials containing a crack parallel to the free surface based on the fractional heat conduction theory.

Considering that cylindrical composites under thermal loading conditions have significant engineering applications, the thermal analysis of the composite structures with cracks is of great importance for the safety design. The classical Fourier heat conduction model implies that the thermal wave can propagate instantaneously in the media at an infinite speed, which contradicts physical facts. For crack problems, the application of non-Fourier heat conduction models on homogeneous materials has been reported in some recent literatures [23–27]. Hu and Chen [25] investigated a partially, thermally insulated crack in an elastic strip under a thermal impact loading and studied the possible crack kinking phenomena. Wang [26] considered the transient thermal cracking associated with non-classical heat conduction in a cylindrical coordinate system. Hu and Chen [28] analyzed the transient heat conduction of a cracked half-plane using dual-phase-lag (DPL) theory. The fracture behavior of a thermoelastic cylinder subjected to a sudden temperature change on its outer surface has been studied by Fu et al. [27] using the hyperbolic heat conduction model. The fractional calculus has been introduced into the hyperbolic heat conduction model to investigate the fracture problem of a circumferential crack in a hollow cylinder under thermal shock by Zhang and Li [29]. Yang and Chen [30] established a thermoelastic model for a functionally graded half-plane containing a crack under thermal shock loading in the framework of hyperbolic heat conduction theory.

To the authors' best knowledge, the thermal problem of a cylindrical crack in a functionally graded cylinder has not been solved due to the mathematical complexity involved. This work is dedicated to obtain the dynamic thermal responses of an FG cylinder containing a cylindrical crack under thermal shock using non-Fourier heat conduction models. The Fourier transform and Laplace transform are applied, and the crack problem is reduced to solving a singular integral equation in the Laplace domain. Then the heat flux intensity factor (HFIF) and temperature field are obtained by applying the numerical Laplace inversion technique. Finally, the effects of heat conduction model, functionally graded parameter, and thermal resistance of crack on the temperature field and HFIF are analyzed numerically.

2. Problem Formulation

As illustrated in Figure 1, an FG hollow cylinder located in the cylindrical coordinate $O - r\varphi z$ is subjected to transient thermal loadings on its inner and outer surfaces. The infinitely long, rigid cylinder has an inner radius R_i, and outer radius R_o, while an axisymmetric, cylindrical crack spreads along the plane $r = R_c$ with the size of $-c < z < c$. For simplicity, the thermal

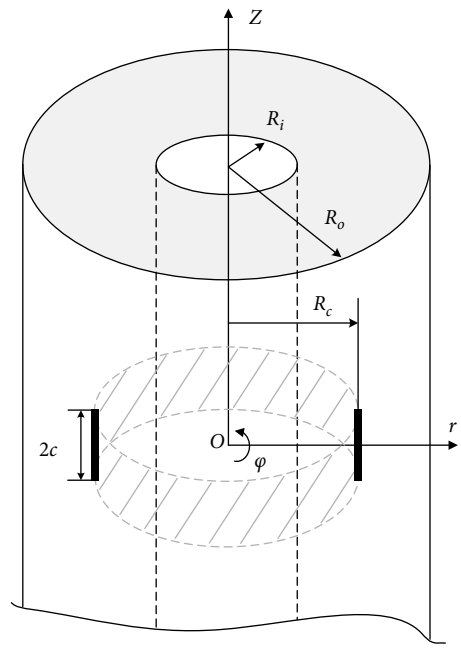

Figure 1: An infinitely long, FG hollow cylinder with a cylindrical crack.

conductivity and mass density of the cylinder are assumed to be radial-coordinate-dependent, while other material properties are homogeneous. The non-Fourier heat conduction model is adopted to analyze the thermal behavior of the cracked FG cylinder with uniform initial temperature T_0.

Considering the axisymmetric nature of the cracked cylinder, the heat flux only exists in the radial, and axial directions, and can be expressed within the structure of the DPL model [28] as,

$$\left(1 + \tau_q \frac{\partial}{\partial t} + \frac{1}{2}\tau_q{}^2 \frac{\partial^2}{\partial t^2}\right)\vec{q} = -k\left(1 + \tau_T \frac{\partial}{\partial t}\right)\vec{\nabla} T, \quad (1)$$

in which, $\vec{q}$ is the heat flux vector, t is time, T is temperature, and k is the thermal conductivity. The phase lag of heat flux τ_q and phase lag of temperature gradient τ_T are material properties. By omitting the quadratic term on the left and setting $\tau_T = 0$ in Eq. (1), another frequently-used, non-Fourier heat conduction model proposed by Cattaneo [31] and Vernotte [32] (C–V model), is obtained. Also, setting $\tau_q = 0$ and $\tau_T = 0$ leads to the classical Fourier heat conduction model. The advancement of the DPL heat conduction model has been clarified by predicting the temperature results tested for some materials, such as, processed meat [33]. Phase lags of heat flux and temperature gradient are material-dependent properties and vary from picoseconds for most of the metals [34] to 10^2 s for non-homogeneous materials [33, 35].

Without heat source, the energy conservation equation reads

$$-\vec{\nabla} \cdot \vec{q} = \rho c_P \frac{\partial T}{\partial t}, \quad (2)$$

where ρ and c_P are mass density and specific heat capacity, respectively.

By eliminating the heat flux from Eqs. (1) and (2), the 2D axisymmetric governing equation of temperature is obtained

$$\left(1+\tau_q\frac{\partial}{\partial t}+\frac{1}{2}\tau_q^2\frac{\partial^2}{\partial t^2}\right)\left[\rho(r)c_P\frac{\partial T}{\partial t}\right] = \left(1+\tau_T\frac{\partial}{\partial t}\right)\left[\frac{\partial k}{\partial r}\frac{\partial T}{\partial r}+k(r)\left(\frac{\partial^2}{\partial r^2}+\frac{\partial}{r\partial r}+\frac{\partial^2}{\partial z^2}\right)T\right], \tag{3}$$

where the thermal conductivity and mass density vary with radial coordinate in a power-law form

$$k(r)=k_0\left(\frac{r}{c}\right)^{\eta},\ \rho(r)=\rho_0\left(\frac{r}{c}\right)^{\eta}, \tag{4}$$

in which, k_0 and ρ_0 are reference material properties, and the power exponent η can also be called as FG parameter.

Substitution of Eq. (4) into (3) leads to

$$\left(1+\tau_q\frac{\partial}{\partial t}+\frac{1}{2}\tau_q^2\frac{\partial^2}{\partial t^2}\right)\frac{\partial T}{\partial t} = d_0\left(1+\tau_T\frac{\partial}{\partial t}\right)\left[\frac{\partial^2}{\partial r^2}+(\eta+1)\frac{\partial}{r\partial r}+\frac{\partial^2}{\partial z^2}\right]T, \tag{5}$$

where $d_0=k_0/\rho_0c_p$ is the reference thermal diffusivity.

The boundary conditions for the partially insulated crack can be written as

$$T^{(1)}(R_i,z,t)=T_a(t),\quad |z|<\infty, \tag{6}$$

$$T^{(2)}(R_o,z,t)=T_b(t),\quad |z|<\infty, \tag{7}$$

$$q_r^{(1)}(R_c,z,t)=q_r^{(2)}(R_c,z,t),\quad abs(z)<\infty, \tag{8}$$

$$T^{(1)}(R_c,z,t)=T^{(2)}(R_c,z,t),\quad |z|\geq c, \tag{9a}$$

$$Vq_r^{(1)}(R_c,z,t)=T^{(1)}(R_c,z,t)-T^{(2)}(R_c,z,t),\quad abs(z)<c, \tag{9b}$$

where T and q_r with the superscripts "(1)" and "(2)" represent temperature and heat flux in the area $r<R_c$ and $r>R_c$, respectively. Equations (8)–(9b) describe the thermal condition along the crack plane, while Eqs. (9a) and (9b) is termed as the mixed boundary condition which enhances the complexity of the problem remarkably. When the thermal resistance of the crack V equals 0, the crack will not disturb the temperature field, and a perfectly conductive crack condition arises. When V approaches infinity, there is no heat flux across the insulating crack.

3. Solution Procedure

The following non-dimensional parameters are introduced to simplify the solution procedure:

$$t'=\frac{td_0}{c^2},\ \tau_q'=\frac{\tau_q d_0}{c^2},\ r'=\frac{r}{c},\quad T^{(j)\prime}=\frac{T^{(j)}-T_0}{T_0},\ V'=\frac{Vk_0}{c},\ q^{(j)\prime}=\frac{q^{(j)}c}{k_0T_0}. \tag{10}$$

It is noted that other parameters with the same units as those in Eq. (10) are omitted here for brevity.

Using the parameters in (10), the governing Equation (5) can be normalized as

$$\left(1+\tau_q'\frac{\partial}{\partial t'}+\frac{1}{2}\tau_q'^2\frac{\partial^2}{\partial t'^2}\right)\frac{\partial T^{(j)\prime}}{\partial t'} = \left(1+\tau_T'\frac{\partial}{\partial t'}\right)\left[\frac{\partial^2}{\partial r'^2}+(\eta+1)\frac{\partial}{r'\partial r'}+\frac{\partial^2}{\partial z'^2}\right]T^{(j)\prime},\quad j=1,2. \tag{11}$$

Applying the Laplace transform to the above equation by assuming the zero initial conditions leads to

$$r'^2\frac{\partial^2\tilde{T}^{(j)'}}{\partial r'^2}+(\eta+1)r'\frac{\partial\tilde{T}^{(j)'}}{\partial r'}+r'^2\frac{\partial^2\tilde{T}^{(j)'}}{\partial z'^2}-\lambda_1 r'^2\tilde{T}^{(j)'}=0, \tag{12}$$

in which, $\lambda_1=s\left(1+\tau_q's+(1/2)\tau_q'^2s^2\right)/\left(1+\tau_T's\right)$ and s is the Laplace variable.

Similar normalization and Laplace transformation processes applied to the boundary conditions give,

$$\tilde{T}^{(1)'}(R_i',z',s)=\tilde{T}_a'(s), \tag{13}$$

$$\tilde{T}^{(2)\prime}(R_o',z',s)=\tilde{T}_b'(s), \tag{14}$$

$$\tilde{q}_r^{(1)\prime}(R_c',z',s)=\tilde{q}_r^{(2)\prime}(R_c',z',s), \tag{15}$$

$$\tilde{T}^{(1)\prime}(R_c',z',s)=\tilde{T}^{(2)\prime}(R_c',z',s),\quad |z'|\geq 1, \tag{16a}$$

$$V'\tilde{q}_r^{(1)\prime}(R_c',z',s)=\tilde{T}^{(1)\prime}(R_c',z',s)-\tilde{T}^{(2)\prime}(R_c',z',s),\quad |z'|<1. \tag{16b}$$

Using superposition, the temperature field resulting from differential Equation (12) under the boundaries (13)~(16b) can be the addition of solutions of two subproblems: (P1) inhomogeneous boundary condition applied to the cylinder surfaces with the absence of crack; (P2) homogeneous thermal load applied to the cracked cylinder. For the first problem, the temperature distribution along the axial direction will be uniform. Thus one could have.

P1:

$$r'^2\frac{d^2\tilde{T}_1^{(j)\prime}}{dr'^2}+(\eta+1)r'\frac{d\tilde{T}_1^{(j)\prime}}{dr'}-\lambda_1 r'^2\tilde{T}_1^{(j)\prime}=0,\quad j=1,2, \tag{17}$$

$$\tilde{T}_1^{(1)\prime}(R_i',s)=\tilde{T}_a'(s), \tag{18}$$

$$\tilde{T}_1^{(2)\prime}(R_o',s)=\tilde{T}_b'(s), \tag{19}$$

$$\tilde{q}_{r1}^{(1)\prime}(R_c',s)=\tilde{q}_{r1}^{(2)\prime}(R_c',s), \tag{20}$$

$$\tilde{T}_1^{(1)\prime}(R_c',s)=\tilde{T}_1^{(2)\prime}(R_c',s), \tag{21}$$

and

P2:

$$r'^2\frac{\partial^2\tilde{T}_2^{(j)\prime}}{\partial r'^2}+(\eta+1)r'\frac{\partial\tilde{T}_2^{(j)\prime}}{\partial r'}+r'^2\frac{\partial^2\tilde{T}_2^{(j)\prime}}{\partial z'^2}-\lambda_1 r'^2\tilde{T}_2^{(j)\prime}=0,\quad j=1,2, \tag{22}$$

$$\tilde{T}_2^{(1)\prime}(R_i', z', s) = \tilde{T}_2^{(2)\prime}(R_o', z', s) = 0, \tag{23}$$

$$\tilde{q}_{r2}^{(1)\prime}(R_c', z', s) = \tilde{q}_{r2}^{(2)\prime}(R_c', z', s), \tag{24}$$

$$\tilde{T}_2^{(1)\prime}(R_c', z', s) = \tilde{T}_2^{(2)\prime}(R_c', z', s), \quad |z'| \geq 1, \tag{25a}$$

$$\begin{aligned} &V'\left[\tilde{q}_{r1}^{(1)\prime}(R_c', s) + \tilde{q}_{r2}^{(1)\prime}(R_c', z', s)\right] \\ &\quad = \tilde{T}_2^{(1)\prime}(R_c', z', s) - \tilde{T}_2^{(2)\prime}(R_c', z', s), \quad |z'| < 1, \end{aligned} \tag{25b}$$

The total temperature and heat flux can be easily obtained from $\tilde{T}^{(j)\prime} = \tilde{T}_1^{(j)\prime} + \tilde{T}_2^{(j)\prime}$ and $\tilde{q}_r^{(j)\prime} = \tilde{q}_{r1}^{(j)\prime} + \tilde{q}_{r2}^{(j)\prime}$ after solving the above two problems.

P1 can be directly solved as,

$$\tilde{T}_1^{(j)\prime} = (ir')^{-\eta/2}\left[C_1^{(j)} I_m\left(\sqrt{\lambda_1} r'\right) + C_2^{(j)} K_m\left(\sqrt{\lambda_1} r'\right)\right], \tag{26}$$

$$\begin{aligned} \tilde{q}_{r1}^{(j)\prime} = \lambda_2 (i)^{-\eta/2}\Big\{ & C_1^{(j)}\Big[r'^{\eta/2}\sqrt{\lambda_1} I_{m-1}\left(\sqrt{\lambda_1} r'\right) \\ & -\left(\frac{\eta}{2} + m\right) r'^{\eta/2-1} I_m\left(\sqrt{\lambda_1} r'\right)\Big] \\ & - C_2^{(j)}\Big[r'^{\eta/2}\sqrt{\lambda_1} K_{m-1}\left(\sqrt{\lambda_1} r'\right) \\ & +\left(\frac{\eta}{2} + m\right) r'^{\eta/2-1} K_m\left(\sqrt{\lambda_1} r'\right)\Big]\Big\}, \end{aligned} \tag{27}$$

where, the imaginary number $i = \sqrt{-1}$, $\lambda_2 = -(1 + \tau_T' s)/\left(1 + \tau_q' s + (1/2)\tau_q'^2 s^2\right)$, and $m = |\eta/2|$. $I_m(\,)$ and $K_m(\,)$ represent the m th-order modified Bessel functions of the first and second kinds, respectively. The unknowns $C_1^{(j)}$ and $C_2^{(j)}$ can be obtained from $\tilde{P}\overrightarrow{C} = \overrightarrow{Q}$, in which, $\overrightarrow{C}$ is defined as

$$\overrightarrow{C} = [\, C_1^{(1)} \quad C_2^{(1)} \quad C_1^{(2)} \quad C_2^{(2)} \,]^{\mathrm{T}}, \tag{28}$$

and the non-zero elements of the 4×4 matrix $\tilde{P}$ and 4×1 vector $\overrightarrow{Q}$ are

$$\begin{aligned} &P_{1,1} = (iR_i)^{-\eta/2} I_m\left(\sqrt{\lambda_1} R_i'\right),\ P_{1,2} = (iR_i)^{-\eta/2} K_m\left(\sqrt{\lambda_1} R_i'\right), \\ &P_{2,3} = (iR_o)^{-\eta/2} I_m\left(\sqrt{\lambda_1} R_o'\right),\ P_{2,4} = (iR_o)^{-\eta/2} K_m\left(\sqrt{\lambda_1} R_o'\right), \\ &P_{3,1} = -P_{3,3} = \sqrt{\lambda_1} I_{m-1}\left(\sqrt{\lambda_1} R_c'\right) - \tfrac{\eta/2+m}{R_c'} I_m\left(\sqrt{\lambda_1} R_c'\right), \\ &-P_{3,2} = P_{3,4} = \sqrt{\lambda_1} K_{m-1}\left(\sqrt{\lambda_1} R_c'\right) + \tfrac{\eta/2+m}{R_c'} K_m\left(\sqrt{\lambda_1} R_c'\right), \\ &P_{4,1} = -P_{4,3} = I_m\left(\sqrt{\lambda_1} R_c'\right),\ P_{4,2} = -P_{4,4} = K_m\left(\sqrt{\lambda_1} R_c'\right), \end{aligned} \tag{29}$$

$$Q_1 = \tilde{T}_a'(s),\ Q_2 = \tilde{T}_b'(s). \tag{30}$$

Now, let's turn to solve the mixed-boundary-value problem P2. Applying the Fourier transform to Equation (22) with respect to z' leads to,

$$r'^2 \frac{\partial^2 \bar{\tilde{T}}_2^{(j)\prime}}{\partial r'^2} + (\eta + 1) r' \frac{\partial \bar{\tilde{T}}_2^{(j)\prime}}{\partial r'} - \xi^2 r'^2 \bar{\tilde{T}}_2^{(j)\prime} - \lambda_1 r'^2 \bar{\tilde{T}}_2^{(j)\prime} = 0. \tag{31}$$

The temperature and the heat flux are then obtained as,

$$\begin{aligned} \tilde{T}_2^{(j)\prime} = \frac{1}{2\pi}\int_{-\infty}^{\infty} & (ir')^{-\eta/2}\left[D_1^{(j)} I_m\left(\sqrt{\lambda_3} r'\right)\right. \\ & \left. + D_2^{(j)} K_m\left(\sqrt{\lambda_3} r'\right)\right] e^{i\xi z\prime} d\xi, \end{aligned} \tag{32}$$

$$\begin{aligned} \tilde{q}_2^{(j)\prime} = \frac{1}{2\pi}\int_{-\infty}^{\infty} & \lambda_2 (i)^{-\eta/2}\Big\{ D_1^{(j)}\Big[(r')^{\eta/2}\sqrt{\lambda_3} I_{m-1}\left(\sqrt{\lambda_3} r'\right) \\ & -\left(\frac{\eta}{2} + m\right)(r')^{\eta/2-1} I_m\left(\sqrt{\lambda_3} r'\right)\Big] \\ & - D_2^{(j)}\Big[(r')^{\eta/2}\sqrt{\lambda_3} K_{m-1}\left(\sqrt{\lambda_3} r'\right) \\ & +\left(\frac{\eta}{2} + m\right)(r')^{\eta/2-1} K_m\left(\sqrt{\lambda_3} r'\right)\Big]\Big\} e^{i\xi z\prime} d\xi, \end{aligned} \tag{33}$$

where, $\lambda_3 = \xi^2 + \lambda_1$.

Using the boundary Equations (23) and (24), the unknowns in Eq. (32) are linked as

$$D_1^{(1)} = -\frac{X_2 X_7}{X_1} D_2^{(2)},\ D_2^{(1)} = X_7 D_2^{(2)},\ D_1^{(2)} = -\frac{X_4}{X_3} D_2^{(2)}, \tag{34}$$

in which,

$$\begin{aligned} &X_1 = I_m\left(\sqrt{\lambda_3} R_i'\right),\ X_2 = K_m\left(\sqrt{\lambda_3} R_i'\right), \\ &X_3 = I_m\left(\sqrt{\lambda_3} R_o'\right),\ X_4 = K_m\left(\sqrt{\lambda_3} R_o'\right), \\ &X_5 = R_c'^{(\eta/2)}\sqrt{\lambda_3} I_{m-1}\left(\sqrt{\lambda_3} R_c'\right) \\ &\qquad - \left(\frac{\eta}{2} + m\right) R_c'^{(\eta/2-1)} I_m\left(\sqrt{\lambda_3} R_c'\right), \\ &X_6 = R_c'^{(\eta/2)}\sqrt{\lambda_3} K_{m-1}\left(\sqrt{\lambda_3} R_c'\right) \\ &\qquad + \left(\frac{\eta}{2} + m\right) R_c'^{(\eta/2-1)} K_m\left(\sqrt{\lambda_3} R_c'\right), \\ &X_7 = \frac{(X_4/X_3 + X_6/X_5)}{(X_2/X_1 + X_6/X_5)}. \end{aligned} \tag{35}$$

The only unknown, independent coefficient $D_2^{(2)}$ can be solved from the mixed boundary conditions (25a) and (25b). A function, defined as the gradient of temperature jump, is introduced

$$\Phi(z', s) = \frac{\partial}{\partial z'}\left[\tilde{T}_2^{(1)}(R_c', z', s) - \tilde{T}_2^{(2)\prime}(R_c', z', s)\right]. \tag{36}$$

Equation (36), expressing the axial gradient of temperature jump across the crack faces, serves as a basic function to solve the mixed-boundary-condition problem using the method of singular integral equation. Due to the existence of crack, the temperature along the plane $r = R_c$ jumps in the radial direction within the range of $|z| < c$, while it is continuous within the range of $|z| \geq c$. Thus, the axial gradient of the temperature jump can describe the nature of thermal disturbance caused by the crack in a unified form.

Thus from Eq. (25a), one could have

$$\Phi(z', s) = 0, \quad |z'| \geq 1, \tag{37}$$

$$\int_{-1}^{1}\Phi(z',s)dz'=0,\quad |z'|<1. \tag{38}$$

Eq. (38) is the single-valuedness condition. With the help of Eq. (34), substituting Eq. (32) into Eq. (36) leads to

$$D_2^{(2)}=\frac{(iR_c')^{\eta/2}}{i\xi \mathrm{X}_8}\int_{-1}^{1}\Phi(\varepsilon,s)e^{-i\xi\varepsilon}d\varepsilon, \tag{39}$$

in which, ε is the integral variable and,

$$\mathrm{X}_8=\left(\frac{\mathrm{X}_4}{\mathrm{X}_3}-\frac{\mathrm{X}_2\mathrm{X}_7}{\mathrm{X}_1}\right)I_m\left(\sqrt{\lambda_3}R_c'\right)+(\mathrm{X}_7-1)K_m\left(\sqrt{\lambda_3}R_c'\right). \tag{40}$$

Substituting Eqs. (27), (32)–(34), and (39) into Eq. (25b) results in a singular integral equation

$$\int_{-1}^{1}\Phi(\varepsilon,s)\left[\frac{1}{z'-\varepsilon}+L(z',\varepsilon)\right]d\varepsilon=\frac{\pi H(s)}{\mathrm{X}_\infty}, \tag{41}$$

in which,

$$L(z',\varepsilon)=\int_0^\infty\frac{\mathrm{X}_{11}-\mathrm{X}_\infty}{\mathrm{X}_\infty}\sin[\xi(z'-\varepsilon)]d\xi, \tag{42}$$

$$\mathrm{X}_{11}=\frac{(iR_c')^{\eta/2}\left[-\mathrm{X}_2\mathrm{X}_7\mathrm{X}_9/\mathrm{X}_1+\mathrm{X}_7\mathrm{X}_{10}+(\mathrm{X}_4/\mathrm{X}_3)I_m\left(\sqrt{\lambda_3}R_c'\right)-K_m\left(\sqrt{\lambda_3}R_c'\right)\right]}{\xi\mathrm{X}_8}, \tag{43}$$

$$\begin{aligned}\mathrm{X}_9=&I_m\left(\sqrt{\lambda_3}R_c'\right)-V'\lambda_2R_c'^{\eta}\sqrt{\lambda_3}I_{m-1}\left(\sqrt{\lambda_3}R_c'\right)\\&+V'\lambda_2\left(\frac{\eta}{2}+m\right)R_c'^{\eta-1}I_m\left(\sqrt{\lambda_3}R_c'\right),\end{aligned} \tag{44}$$

$$\begin{aligned}\mathrm{X}_{10}=&K_m\left(\sqrt{\lambda_3}R_c'\right)+V'\lambda_2R_c'^{\eta}\sqrt{\lambda_3}K_{m-1}\left(\sqrt{\lambda_3}R_c'\right)\\&+V'\lambda_2\left(\frac{\eta}{2}+m\right)R_c'^{\eta-1}K_m\left(\sqrt{\lambda_3}R_c'\right),\end{aligned} \tag{45}$$

$$\mathrm{X}_\infty=\lim_{\xi\to\infty}\mathrm{X}_{11}=-\frac{V'\lambda_2}{2}(i)^{\eta/2}(R_c')^{3\eta/2}, \tag{46}$$

$$\begin{aligned}H(s)=V'\lambda_2\Bigg\{&\left[R_c'^{\eta}\sqrt{\lambda_1}I_{m-1}\left(\sqrt{\lambda_1}R_c'\right)\right.\\&\left.-\left(\frac{\eta}{2}+m\right)R_c'^{\eta-1}I_m\left(\sqrt{\lambda_1}R_c'\right)\right]C_1^{(1)}\\&-\left[R_c'^{\eta}\sqrt{\lambda_1}K_{m-1}\left(\sqrt{\lambda_1}R_c'\right)\right.\\&\left.+\left(\frac{\eta}{2}+m\right)R_c'^{\eta-1}K_m\left(\sqrt{\lambda_1}R_c'\right)\right]C_2^{(1)}\Bigg\}.\end{aligned} \tag{47}$$

The fundamental solution of the singular integral equation (41) under the single-valuedness condition (38) is [36],

$$\Phi(\varepsilon,s)=f(\varepsilon,s)\left(1-\varepsilon^2\right)^{-1/2}. \tag{48}$$

Eqs. (41) and (38) can be solved numerically by adopting the Gauss–Jacobi integration formulas in [37] as,

$$\sum_{\mu=1}^{N}\frac{1}{N}f\left(\varepsilon_\mu,s\right)\left[\frac{1}{z_\omega'-\varepsilon_\mu}+L\left(z_\omega',\varepsilon_\mu,s\right)\right]=\frac{H(s)}{\mathrm{X}_\infty}, \tag{49}$$

$$\sum_{\mu=1}^{N}f\left(\varepsilon_\mu,s\right)=0, \tag{50}$$

in which,

$$\varepsilon_\mu=\cos\left(\frac{2\mu-1}{2N}\pi\right),\quad \mu=1,2,\ldots,N, \tag{51}$$

$$z_\omega'=\cos\left(\frac{\omega}{N}\pi\right),\quad \omega=1,2,\ldots,N-1. \tag{52}$$

After calculating the function $f(\varepsilon,s)$ numerically, the four unknown coefficients $D_1^{(j)}$ and $D_2^{(j)}$ can be obtained from Eqs. (34), (39), and (48). Finally, problem P2 is solved.

4. Temperature Field and Heat Flux Intensity Factor

The total temperature in the cylinder can be obtained by adding Equations (29)–(35) as,

$$\begin{aligned}\tilde{T}^{(j)\prime}=&(ir')^{-\eta/2}\left[C_1^{(j)}I_m\left(\sqrt{\lambda_1}r'\right)+C_2^{(j)}K_m\left(\sqrt{\lambda_1}r'\right)\right]\\&+\frac{1}{2\pi}\int_{-\infty}^{\infty}(ir')^{-\eta/2}\left[D_1^{(j)}I_m\left(\sqrt{\lambda_3}r'\right)\right.\\&\left.+D_2^{(j)}K_m\left(\sqrt{\lambda_3}r'\right)\right]e^{i\xi z'}d\xi,\quad j=1,2,\end{aligned} \tag{53}$$

in which, $D_1^{(1)}$, $D_2^{(1)}$, and $D_1^{(2)}$ are expressed in terms of $D_2^{(2)}$, while $D_2^{(2)}$ can be numerically obtained from Eq. (42) using the Gauss–Chebyshev integration equation

$$\begin{aligned}D_2^{(2)}&=-\frac{(iR_c')^{\eta/2}}{\xi\mathrm{X}_8}\int_{-1}^{1}\Phi(\varepsilon,s)\sin(\xi\varepsilon)d\varepsilon\\&=-\frac{(iR_c')^{\eta/2}}{\xi\mathrm{X}_8}\sum_{\mu=1}^{N}\frac{\pi}{N}f\left(\varepsilon_\mu,s\right)\sin\left(\xi\varepsilon_\mu\right).\end{aligned} \tag{54}$$

The concept of heat flux intensity factor (HFIF), similar to the stress intensity factor, is introduced to describe the heat gathering degree around the crack tip

$$K_q(t)=\lim_{z\to c}\sqrt{2(z-c)}q_r^{(2)}(R_c,z,t). \tag{55}$$

Using the parameter $K_q'=K_q\sqrt{c}/(k_0T_0)$, the non-dimensional HFIF in the Laplace domain is written as

$$\tilde{K}_q'(s)=\lim_{z'\to1}\sqrt{2(z'-1)}\tilde{q}_r^{(2)\prime}(R_c',z',s). \tag{56}$$

Substituting Eqs. (30) and (36) into the above equation, one could have

$$\tilde{K}_q'(s)=\frac{\lambda_2}{2}R_c'^{\eta}f(1,s), \tag{57}$$

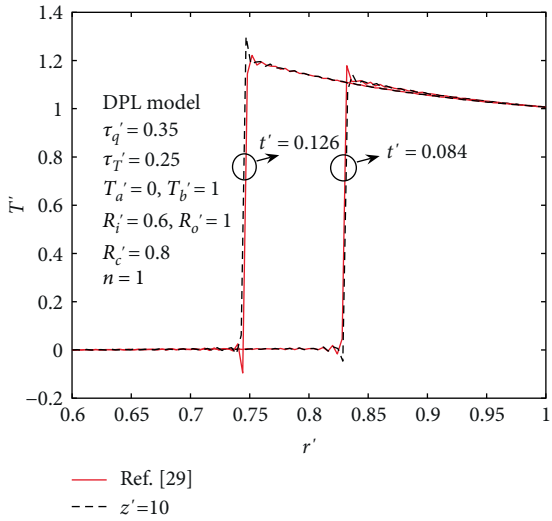

Figure 2: Comparison of temperature distribution away from the crack with the result in [39].

in which, $f(1, s)$ is calculated from $f(\varepsilon_\mu, s)$ using the interpolation method.

Finally, the transient temperature and HFIF in the time domain are obtained by applying the numerical Laplace inversion technique described in [38] to Eqs. (56) and (60), respectively.

5. Numerical Results

In this section, a fiber reinforced composite cylinder containing a cylindrical crack is taken as an example to demonstrate the applicability of the mathematical model proposed in this paper. A sudden temperature change is applied on the inner surface of cylinder, and transient temperature field and HFIF are obtained based on the DPL heat conduction model. The effects of heat conduction model and phase lags, FG parameter, and thermal resistance of crack on the results are analyzed in detail. In the meanwhile, the solution procedure is verified in Section 5.1 with the temperature result presented in [39] which described the non-Fourier heat conduction in uncracked FG cylinders.

5.1. Validation of the Solution Procedure. In order to justify the solution process in this paper, a cracked FG cylinder with the same configuration and temperature loading as the uncracked cylinder in [39] is taken for illustration. The mass density and thermal conductivity vary with the radial coordinate gradually with $n = 1$, while other parameters are homogeneous. The crack spreads along the plane $R_c' = 0.8$ and has the non-dimensional length $-1 < z' < 1$. It is known from the Saint-Venant principle that the temperature field near the crack will be disturbed and not be affected by the crack at a position far away from it. Thus, the temperature field far from the crack should be the same as that for uncracked cylinders. The temperature distributions along the radial direction at $z' = 10$ are drawn in Figure 2 and compared with the results of uncracked cylinder at two different instants $t' = 0.084$ and $t' = 0.126$. It is seen that the thermal wave propagates from the outer surface of the cylinder to the inner surface under the DPL heat conduction model. Evidently, the difference between the transient temperature field away from the cylindrical crack obtained in this paper and that in the reference for uncracked cylinder is negligible, which proves the correctness of the solution procedure.

Table 1: Reference material properties.

ρ_0 (Kg/m^3)	c_P (J/KgK)	k_0 (W/mK)	τ_q (s)	τ_T (s)
1302	1006	11.6	0.8	0.6

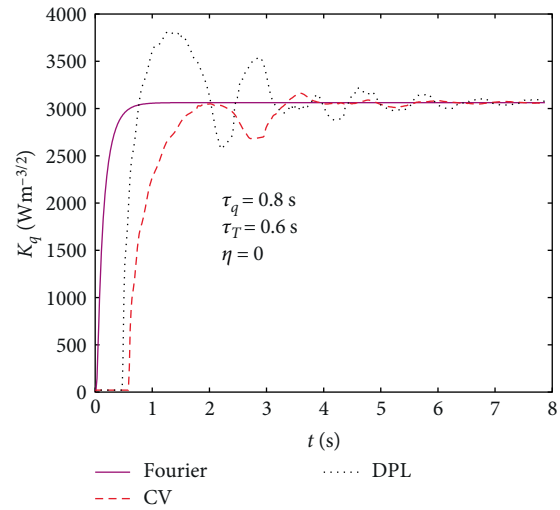

Figure 3: Effect of heat conduction model on HFIF for a homogeneous cylinder.

5.2. Effect of Heat Conduction Model and Phase Lag Parameters. In this subsection and thereafter, a cylinder with the size of $R_i = 0.006$ m and $R_o = 0.01$ m containing a cylindrical crack of length $2c$ at $R_c = 0.008$ m is chosen for the parameter analyses. The cylinder is made of carbon fiber reinforced resin matrix composite, and the reference properties are chosen with 20% volume fraction of fiber, shown in Table 1. It should be noted that the phase lag of heat flux is chosen referring to [40], and the phase lag of temperature gradient is assumed correspondingly due to the absence of this value in literature. The crack length is $2c = 0.006$ m. The inner surface of the cylinder is heated to $T_a = 330$ K suddenly, while the outer surface is kept at the initial temperature $T_0 = 300$ K. The effects of heat conduction model and corresponding phase lags on the transient heat flux intensity factor and temperature field are analyzed in this subsection.

The histories of HFIF calculated based on different heat conduction models for a homogeneous cylinder with an insulated cylindrical crack are depicted in Figure 3. As the HFIF represents the degree of heat concentration around the crack tip, a higher value of HFIF means a more dangerous thermal situation. It can be seen from Figure 3 that the value of K_q at stable state is the same for all the heat conduction theories, however, the maximum value of K_q strongly depends on the heat conduction theory adopted. Compared to the HFIF

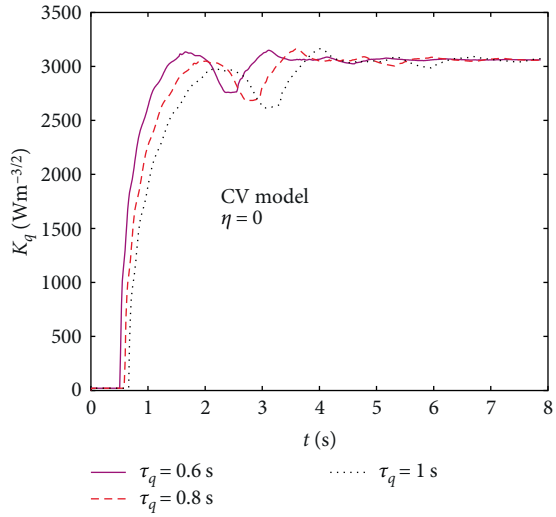

Figure 4: Effect of τ_q on HFIF for a homogeneous cylinder based on the C–V model.

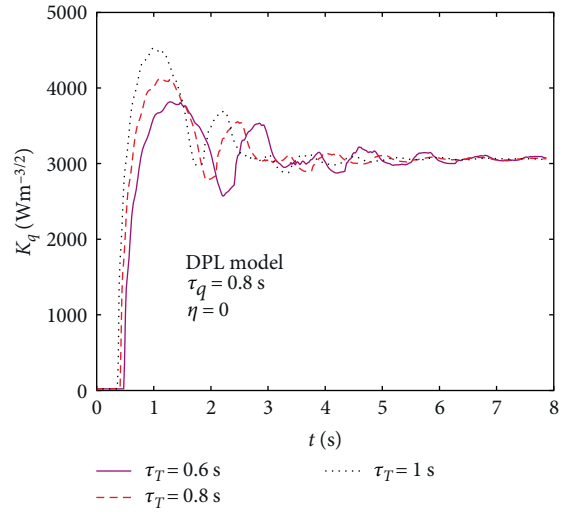

Figure 6: Effect of τ_T on HFIF for a homogeneous cylinder based on the DPL model.

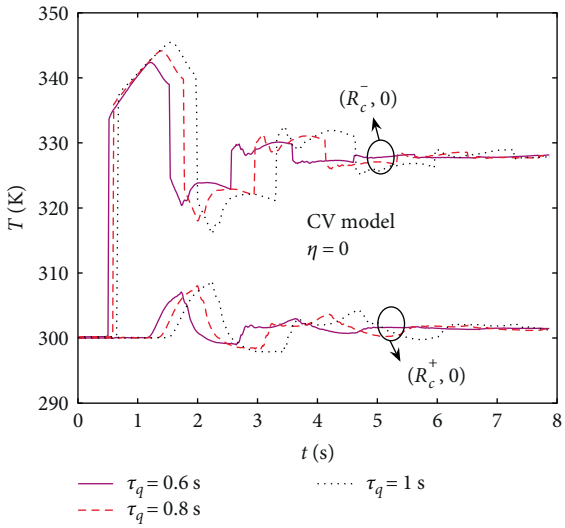

Figure 5: Effect of τ_q on the temperature history at crack face midpoints for a homogeneous cylinder based on the C–V model.

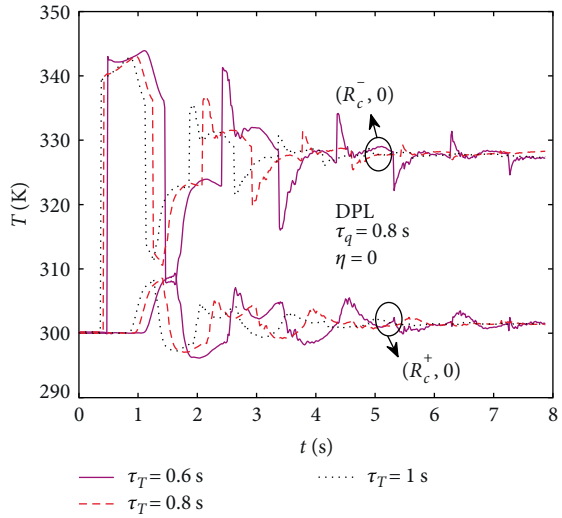

Figure 7: Effect of τ_T on the temperature history at crack face midpoints for a homogeneous cylinder based on the DPL model.

history obtained by the Fourier model, K_q oscillates first and has a higher maximum value for non-Fourier models. Also, the DPL model induces a higher K_q than the C–V model, which declares the importance of DPL heat conduction model to predict the thermal concentration degree around the crack.

The effect of phase lag of heat flux τ_q on the HFIF history and temperature histories of the crack face midpoints of a homogeneous cylinder are shown in Figures 4 and 5, respectively. Three different values of $\tau_q = 0.6$ s, 0.8 s, 1.0 s within the structure of C–V model are chosen for the analysis. It can be seen from Figure 4 that the increase of τ_q raises the oscillation range of HFIF, while its influence on the maximum value of HFIF is indiscernible. Figure 5 clearly shows the temperature jump across the crack faces, and the temperature at the inner crack face is much higher than that at the outer crack face. Due to the existence of the insulated crack, the thermal wave will be reflected back when it propagates from the inner surface to the outer surface. Then, more heat is gathered around the inner crack face, and the temperature is elevated substantially to a value higher than the applied loading T_a. Similar to the conclusion given by Akbarzadeh and Chen [39], the increase of τ_q delays the start signal of the thermal wave and increases the maximum temperature of the two crack faces.

Figures 6 and 7 illustrate the effect of phase lag of temperature gradient τ_T on the transient heat flux intensity factor and temperature field, respectively, within the structure of DPL heat conduction model. The cylinder is taken to be homogeneous, while the phase lag of heat flux is kept constant at $\tau_q = 0.8$ s and τ_T is assumed to vary from 0.6 s to 1.0 s. Different from the effect of τ_q on the maximum K_q in Figure 4, the increase of τ_T generally elevates the maximum value of HFIF, which is clearly shown in Figure 6. It reveals that a cracked

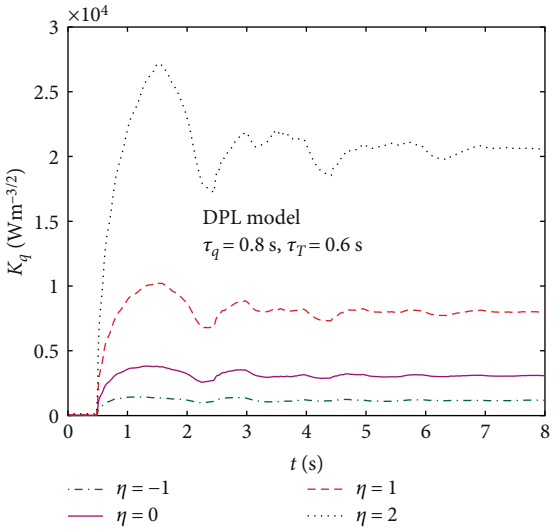

Figure 8: Effect of FG parameter on HFIF based on the DPL model.

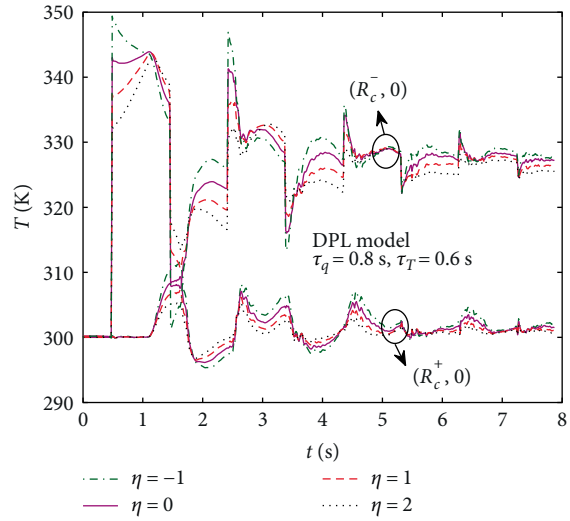

Figure 9: Effect of FG parameter on the temperature history at crack face midpoints based on the DPL model.

structure made of a material with a higher τ_T is more dangerous under sudden temperature change. By comparing Figures 5 and 7, the temperature at crack face midpoints obtained using the DPL model needs more time to get stable than that using the C–V model. Moreover, the influence of τ_T on the maximum temperature is not obvious.

5.3. Effect of FG Parameter. The thermal conductivity and mass density of cylinder vary with the radial coordinate in a power-law form as shown in Eq. (4), while other parameters are homogeneous. Different values of FG parameter (power exponent) correspond to a cylinder made of materials with different properties, thus affects the thermal responses remarkably. In this subsection, the effects of FG parameter η on the HFIF history, temperature history of crack face midpoints, and temperature distribution along the crack plane are shown in Figures 8~10, respectively. It is worth mentioning that the DPL heat conduction model is taken for the thermal analyses.

It can be seen from Figure 8 that the rise of inhomogeneous degree increases the heat flux intensity factor entirely, including the oscillation range, maximum value, and the stable value. This reveals that the employment of inhomogeneous cylinders with positive FG parameter is more thermally dangerous than the homogeneous ones. Meanwhile, an inhomogeneous cylinder with negative FG parameter can serve as a nice thermal barrier structure as it reduces the thermal concentration degree around the crack remarkably. Different from the situation of HFIF history, the effect of FG parameter η on the temperature history of midpoints of crack faces is weak, which is depicted in Figure 9. Due to the use of DPL heat conduction model, the temperature jump across the crack faces shows clear oscillation behavior. The temperature jump is more obvious in Figure 10, which illustrates the temperature distribution along the crack plane at a specific instant $t = 0.784$ s for different FG parameters. Clearly, the temperature at one crack face differs from another within the range of crack $-0.003\text{ m} < z < 0.003$ m, and this phenomenon becomes

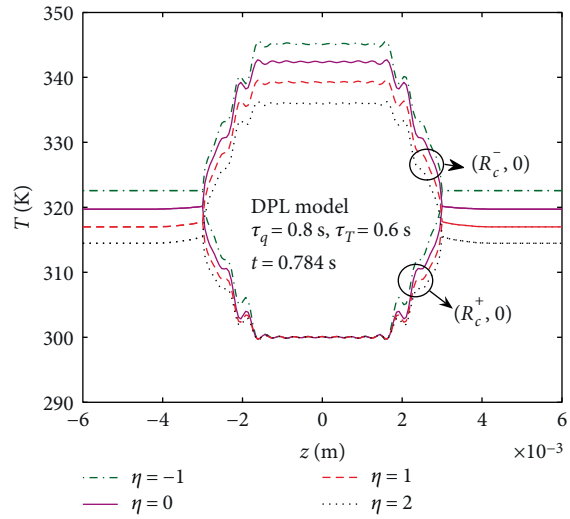

Figure 10: Effect of FG parameter on the temperature distribution along the crack plane based on the DPL model.

continuously beyond this range. Also, the temperature at the inner crack face is much higher than that at the outer crack face due to the outwards thermal flow direction. Figure 10 also indicates that η has sensible effect on the temperature of inner crack face and negligible effect on the temperature of the outer crack face, as the thermal wave has not arrived at the outer crack face at the instant $t = 0.784$ s due to the thermal reflection by the insulated crack face.

5.4. Effect of Thermal Resistance of Crack. The effect of thermal resistance of crack V on the transient HFIF and temperature field of crack face midpoints are shown in Figures 11 and 12, respectively. The cylinder is taken to be inhomogeneous with $\eta = 1$, and the thermal results are obtained based on the DPL model. As stated previously, an infinitely large value of V corresponds to an insulated crack, while two other

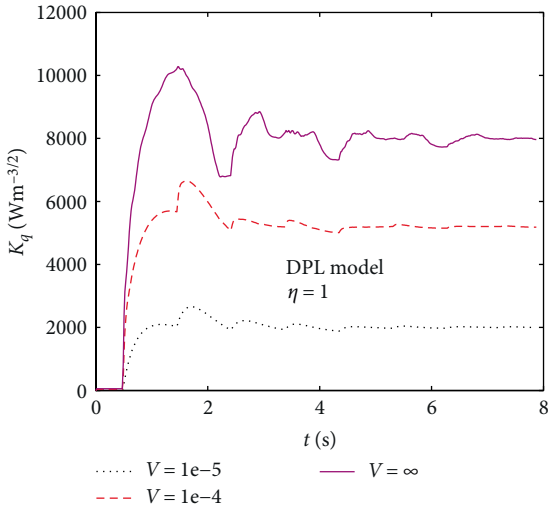

Figure 11: Effect of thermal resistance of crack on HFIF of nonhomogeneous cylinder with $\eta = 1$ based on the DPL model.

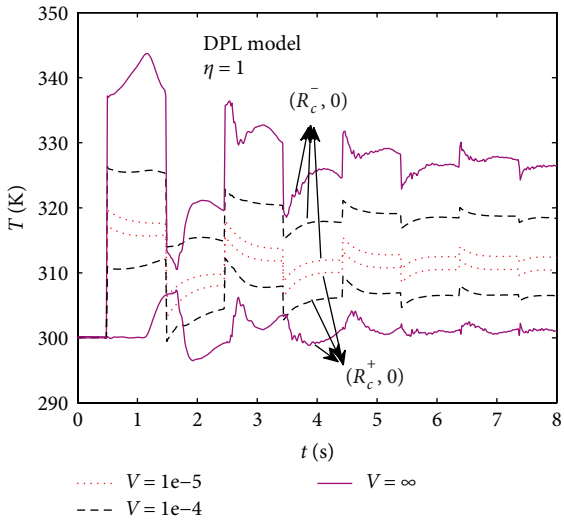

Figure 12: Effect of thermal resistance of crack on the temperature history at crack face midpoints of nonhomogeneous cylinder with $\eta = 1$ based on the DPL model.

partially insulated cracks with $V = 1 \times 10^{-4}\,\mathrm{km}^2\,\mathrm{sJ}^{-1}$ and $V = 1 \times 10^{-5}\,\mathrm{km}^2\,\mathrm{sJ}^{-1}$ are chosen for analysis.

With the decrease of V, the crack tends to be thermally conductive. As shown in Figure 11, a smaller value of thermal resistance of crack leads to a lower HFIF, which indicates that a crack with higher conductivity leads to a lower heat concentration degree at the crack tip. According to the temperature history shown in Figure 12, the temperature jump across crack face shrinks with the decrease of V. Clearly, the temperature difference between the two crack faces of the insulating crack ($V = \infty$) is much higher than that of the nearly conducting crack ($V = 1 \times 10^{-5}\,\mathrm{km}^2\,\mathrm{sJ}^{-1}$) for the whole dynamic equilibrium process. Similar conclusions have been reported by Hu and Chen [28]. It is also obvious that the temperature oscillates first and tends to be steady because of the significant non-Fourier thermal effect.

6. Conclusion

The transient heat conduction of a functionally graded cylinder containing a cylindrical crack is investigated in this paper using the non-Fourier heat conduction theory. The mixed-boundary-value problem is solved with the employment of the singular integral equation and Laplace transform methods. The concept of heat flux intensity factor is introduced to evaluate the heat concentration degree at the crack tip. Finally, the effects of heat conduction model, FG parameter, and thermal resistance of the crack on the transient HFIF and temperature field are analyzed numerically.

It is found that the temperature field across the two crack faces is discontinuous due to the existence of insulating crack. The heat conduction models adopted and related phase lags have great effects on the thermal responses. Due to the use of non-Fourier models, the HFIF are elevated remarkably, and the temperature shows significant oscillation behavior. Within the structure of FG profile used in this paper, an inhomogeneous cylinder with negative FG parameter can serve as a better thermal barrier structure than the homogeneous one. Also, the thermal resistance of crack is an important parameter which reduces the HFIF and temperature jump across the crack faces when the crack becomes more conductive.

Data Availability

The data used to support the findings of this study are included within the article.

Conflicts of Interest

The authors declare that they have no conflicts of interest.

Acknowledgments

This work is partially supported by the National Natural Science Foundation of China (grant number 11702137), Natural Science Foundation of Jiangsu Province of China (grant number BK20170816), and the Fundamental Research Funds for the Central Universities (grant number 309171B8802).

References

[1] Y.-D. Li, H. Zhao, and T. Xiong, "The cylindrical interface crack in a layered tubular composite of finite thickness under torsion," *European Journal of Mechanics–A/Solids*, vol. 39, pp. 113–119, 2013.

[2] Y. Miyamoto, W. A. Kaysser, B. H. Rabin, A. Kawasaki, and R. G. Ford, *Functionally Graded Materials: Design, Processing and Applications*, Kluwer Academic Publishers, Boston, 1999.

[3] R. M. Mahamood and E. T. Akinlabi, *Functionally Graded Materials*, Springer, Switzerland, 2017.

[4] H. G. Fu, Q. Xiao, and J. D. Xing, "A study on the crack control of a high-speed steel roll fabricated by a centrifugal casting technique," *Materials Science and Engineering: A*, vol. 474, no. 1-2, pp. 82–87, 2008.

[5] Z. P. Zhou, L. Huang, Y. J. Shang, Y. P. Li, L. Jiang, and Q. Lei, "Causes analysis on cracks in nickel-based single crystal superalloy fabricated by laser powder deposition additive manufacturing," *Materials & Design*, vol. 160, pp. 1238–1249, 2018.

[6] Y. D. Li and K. Y. Lee, "Fracture analysis on the arc-shaped interface in a layered cylindrical piezoelectric sensor polarized along its axis," *Engineering Fracture Mechanics*, vol. 76, no. 13, pp. 2065–2073, 2009.

[7] H. M. Zbib, J. P. Hirth, and I. Demir, "The stress intensity factor of cylindrical cracks," *International Journal of Engineering Science*, vol. 33, no. 2, pp. 247–253, 1995.

[8] L. C. Guo, L. Z. Wu, T. Zeng, and L. Ma, "Mode I crack problem for a functionally graded orthotropic strip," *European Journal of Mechanics–A/Solids*, vol. 23, no. 2, pp. 219–234, 2004.

[9] W. Z. Yang and Z. T. Chen, "Thermo-viscoelastic response of a cracked, functionally graded half-plane under a thermal shock," *Engineering Fracture Mechanics*, vol. 206, pp. 267–277, 2019.

[10] G. Bao and L. Wang, "Multiple cracking in functionally graded ceramic/metal coatings," *International Journal of Solids and Structures*, vol. 32, no. 19, pp. 2853–2871, 1995.

[11] H. J. Choi, T. E. Jin, and K. Y. Lee, "Collinear cracks in a layered half-plane with a graded non-homogeneous interfacial zone – part II: thermal response," *International Journal of Fracture*, vol. 94, no. 2, pp. 123–135, 1998.

[12] H. J. Choi, K. Y. Lee, and T. E. Jin, "Collinear cracks in a layered half-plane with a graded non-homogeneous interfacial zone – part I: mechanical response," *International Journal of Fracture*, vol. 94, no. 2, pp. 103–122, 1998.

[13] Z. H. Jin and N. Noda, "Transient thermal stress intensity factors for a crack in a semi-infinite plate of a functionally gradient material," *International Journal of Solids and Structures*, vol. 31, no. 2, pp. 203–218, 1994.

[14] F. Erdogan and B. H. Wu, "The surface crack problem for a plate with functionally graded properties," *Journal of Applied Mechanics*, vol. 64, no. 3, pp. 449–456, 1997.

[15] P. Gu and R. J. Asaro, "Cracks in functionally graded materials," *International Journal of Solids and Structures*, vol. 34, no. 1, pp. 1–17, 1997.

[16] Z. H. Jin, "Crack-tip singular fields in functionally graded materials," in *Encyclopedia of Thermal Stresses*, R. B. Hetnarski, Ed., pp. 798–805, Springer, Dordrecht, 2014.

[17] C. Y. Li and G. J. Weng, "Dynamic stress intensity factor of a cylindrical interface crack with a functionally graded interlayer," *Mechanics of Materials*, vol. 33, no. 6, pp. 325–333, 2001.

[18] Z. H. Jin and G. H. Paulino, "A viscoelastic functionally graded strip containing a crack subjected to in-plane loading," *Engineering Fracture Mechanics*, vol. 69, no. 14–16, pp. 1769–1790, 2002.

[19] W. J. Feng, R. K. L. Su, and Z. Q. Jiang, "Torsional impact response of a cylindrical interface crack between a functionally graded interlayer and a homogeneous cylinder," *Composite Structures*, vol. 68, no. 2, pp. 203–209, 2005.

[20] Z. Q. Cheng, S. A. Meguid, and Z. Zhong, "Thermo-mechanical behavior of a viscoelastic FGMs coating containing an interface crack," *International Journal of Fracture*, vol. 164, no. 1, pp. 15–29, 2010.

[21] P. P. Shi, "Cylindrical interface crack in a hollow layered functionally graded cylinder under static torsion," *Mechanics Based Design of Structures and Machines*, vol. 44, no. 3, pp. 250–269, 2016.

[22] X. Y. Zhang, Y. J. Xie, and X. F. Li, "Transient thermoelastic response in a cracked strip of functionally graded materials via generalized fractional heat conduction," *Applied Mathematical Modelling*, vol. 70, pp. 328–349, 2019.

[23] Z. T. Chen and K. Q. Hu, "Thermo-elastic analysis of a cracked half-plane under a thermal shock impact using the hyperbolic heat conduction theory," *Journal of Thermal Stresses*, vol. 35, no. 4, pp. 342–362, 2012.

[24] Z. T. Chen and K. Q. Hu, "Thermoelastic analysis of a cracked substrate bonded to a coating using the hyperbolic heat conduction theory," *Journal of Thermal Stresses*, vol. 37, no. 3, pp. 270–291, 2014.

[25] K. Q. Hu and Z. T. Chen, "Thermoelastic analysis of a partially insulated crack in a strip under thermal impact loading using the hyperbolic heat conduction theory," *International Journal of Engineering Science*, vol. 51, pp. 144–160, 2012.

[26] B. L. Wang, "Transient thermal cracking associated with non-classical heat conduction in cylindrical coordinate system," *Acta Mechanica Sinica*, vol. 29, no. 2, pp. 211–218, 2013.

[27] J. W. Fu, Z. T. Chen, L. F. Qian, and K. Q. Hu, "Transient thermoelastic analysis of a solid cylinder containing a circumferential crack using the C–V heat conduction model," *Journal of Thermal Stresses*, vol. 37, no. 11, pp. 1324–1345, 2014.

[28] K. Q. Hu and Z. T. Chen, "Transient heat conduction analysis of a cracked half-plane using dual-phase-lag theory," *International Journal of Heat and Mass Transfer*, vol. 62, pp. 445–451, 2013.

[29] X. Y. Zhang and X. F. Li, "Transient thermal stress intensity factors for a circumferential crack in a hollow cylinder based on generalized fractional heat conduction," *International Journal of Thermal Sciences*, vol. 121, pp. 336–347, 2017.

[30] W. Z. Yang and Z. T. Chen, "Investigation of the thermal-elastic problem in cracked semi-infinite FGM under thermal shock using hyperbolic heat conduction theory," *Journal of Thermal Stresses*, vol. 42, no. 8, pp. 993–1010, 2019.

[31] C. Cattaneo, "A form of heat conduction equation which eliminates the paradox of instantaneous propagation," *Compte Rendus*, vol. 247, no. 4, pp. 431–433, 1958.

[32] P. Vernotte, "Some possible complications in the phenomena of thermal conduction," *Compte Rendus*, vol. 252, pp. 2190–2191, 1961.

[33] P. J. Antaki, "New interpretation of non-Fourier heat conduction in processed meat," *Journal of Heat Transfer-Transactions of the ASME*, vol. 127, no. 2, pp. 189–193, 2005.

[34] D. Y. Tzou, *Macro- to Microscale Heat Transfer: The Lagging Behavior*, John Wiley & Sons, United Kingdom, 2nd edition, 2015.

[35] W. Roetzel, N. Putra, and S. K. Das, "Experiment and analysis for non-Fourier conduction in materials with non-homogeneous inner structure," *International Journal of Thermal Sciences*, vol. 42, no. 6, pp. 541–552, 2003.

[36] F. Erdogan, G. D. Gupta, and T. S. Cook, "Numerical solution of singular integral equations," in *Mechanics of Fracture, Volume 1: Methods of Analysis and Solutions of Crack Problems*, G. C. Sih, Ed., pp. 368–425, Noordhoff, Leyden, Netherlands, 1973.

[37] J. W. Fu, Z. T. Chen, L. F. Qian, and Y. D. Xu, "Non-Fourier thermoelastic behavior of a hollow cylinder with an embedded or edge circumferential crack," *Engineering Fracture Mechanics*, vol. 128, pp. 103–120, 2014.

[38] F. Durbin, "Numerical inversion of Laplace transforms: an efficient improvement to Dubner and Abate's method," *The Computer Journal*, vol. 17, no. 4, pp. 371–376, 1974.

[39] A. Akbarzadeh and Z. Chen, "Heat conduction in one-dimensional functionally graded media based on the dual-phase-lag theory," *Proceedings of the Institution of Mechanical Engineers, Part C: Journal of Mechanical Engineering Science*, vol. 227, no. 4, pp. 744–759, 2013.

[40] L. C. Zhou, J. S. Lin, H. F. Lin, and G. H. Chen, "Electrical-thermal switching effect in high-density polyethylene/graphite nanosheets conducting composites," *Journal of Materials Science*, vol. 43, no. 14, pp. 4886–4891, 2008.